Journal of Saudi Chemical Society (2016) **xxx**, xxx–xxx

King Saud University

Journal of Saudi Chemical Society

www.ksu.edu.sa
www.sciencedirect.com

ORIGINAL ARTICLE

Synthesis, spectroscopic, structural and thermal characterizations of $[(C_7H_6NO_4)_2TeBr_6{\cdot}4H_2O]$

S. Smaoui [a,*], **A. Kabadou** [a], **A. Van Der Lee** [b], **A. Ben Salah** [a], **M. Abdelmouleh** [a]

[a] *Laboratoire des Sciences des Matériaux et de l'Environnement, Faculté des Sciences de Sfax Université de, Sfax 3018, Tunisia*
[b] *Institut Européen des Membranes (UMR 5635), Université de Montpellier II, cc 047, Place E. Montpellier, France*

Received 23 November 2015; revised 5 February 2016; accepted 7 February 2016

KEYWORDS

Inorganic–organic compounds;
Crystal structure;
IR-Raman spectroscopy;
Thermal analysis;
Optical properties

Abstract Tellurium (IV) complexes with pyridine-2,6-dicarboxylate ligand were synthesized by slow evaporation from aqueous solutions yielding a new compound: $[(C_7H_6NO_4)_2TeBr_6{\cdot}4H_2O]$. The structure of this compound was solved and refined by single-crystal X-ray diffraction. The compound is centrosymmetric $P2_1/c$ (N°: 14) with the parameters a = 8.875(5) Å, b = 15.174(5) Å, c = 10.199(5) Å, β = 94.271° (5) and Z = 2. The structure consists of isolated H_2O, isolated $[TeBr_6]^{2-}$ octahedral anions and (pyridine-2,6-dicarboxylate) $[C_7H_6NO_4]^+$ cations. The stability of the structure was ensured by ionic and hydrogen bonding contacts (N–H···Br and O–H···Br) and Van-Der Walls interaction. The thermal decomposition of the compound was studied by thermogravimetric analysis (TGA) and differential scanning calorimetry (DSC). The FTIR and Raman spectroscopy at different temperatures confirm the existence of vibrational modes that correspond to the organic, inorganic and water molecular groups. Additionally, the UV–Vis diffuse reflectance spectrum was recorded in order to investigate the band gap nature. The measurements show that this compound exhibits a semiconducting behavior with an optical band gap of 2.66 eV.

1. Introduction

Design and synthesis of organic–inorganic hybrid solids, based on the concept of crystal engineering, have attracted much attention in organic–inorganic hybrid materials and supramolecular chemistry because of their magnetic, electronic and optical properties as well as the possibility of changing both its coordination geometry and functional properties by the variation of organic components and metal ions [1–7].

Research in the field of organic–inorganic hybrid materials with pyridine and its derivatives as templating agents has led to some materials with interesting physical properties [8–10].

Pyridine-2,6-dicarboxylic acid (pydc-2,6) forms stable chelates with simple metal ions and oxometal cations and can display a widely varying coordination behavior, functioning as a multidentate ligand. Dipicolinates (dipic) commonly generate transition metals by either carboxylate bridges between metal centers, to form polymeric, dimeric complexes [11–13], or by tridentate (O, N, O') chelation to one metal ion [14–15].

* Corresponding author.
E-mail address: sameh.smaoui.belguith@gmail.com (S. Smaoui).
Peer review under responsibility of King Saud University.

ELSEVIER Production and hosting by Elsevier

http://dx.doi.org/10.1016/j.jscs.2016.02.002

Please cite this article in press as: S. Smaoui et al., Synthesis, spectroscopic, structural and thermal characterizations of $[(C_7H_6NO_4)_2TeBr_6{\cdot}4H_2O]$, Journal of Saudi Chemical Society (2016), http://dx.doi.org/10.1016/j.jscs.2016.02.002

This work is part of a larger project involving studies of the crystal structure in the hexahalogenometallate family with relatively organic cations [16–19]. The compounds with hexahalogeno-complexes and the general formula $A_2M'X_6$ (where A is an alkali) have the K_2PtCl_6 structure [20–26]. For example, the compound $(NH_4)_2TeBr_6$ crystallizes in the cubic K_2PtCl_6 structure, space group Fm $\overline{3}$ m, with the lattice parameter a = 10.728Å. In this structure, all octahedrals are isolated and regular with a Te–Br distance equal to 2.681(2) Å [27]. Tellurium (IV) reaches its highest coordination number of six in the halide complexes $[TeX_6]^{2-}$ (X = Cl, Br or I) [28–29]. These complexes are tested through a valence shell electron pair repulsion (VSEPR) approach in order to analyze its structure [30,31]. In fact, they have seven pairs of electrons, one of which can be regarded as a lone pair. In association with simple cations, the $[TeX_6]^{2-}$ ions tend to be octahedral, although there are unusual features of the electronic absorption and vibrational spectra which require special treatment [32].

In this paper, we investigate the substitution of the dipicolinic acid molecule in the hexabromotellurate compound family. The synthesis, the structure analysis obtained from the single-crystal data, the spectroscopy, the optical absorption, and the thermal studies of the newhybrid hexabromotellurate complex $[(C_7H_6NO_4)_2TeBr_6{\cdot}4H_2O]$ are reported.

2. Experimental

2.1. Synthesis of crystal sample

The ligand pydc-2,6(0.334 g, 2 mmol) was added to an aqueous solution (10 ml) of TeO_2 (0.1596 g, 1 mmol) in hydrobromic acid at T = 80 °C. The resulting bright red solution was stirred for about 10 min and then left to slowly concentrate by solvent evaporation at room temperature for a period of 4 days. Well-formed, bright red octahedral crystals of the product appeared. They were collected by filtration.

Properties: remarkably stable, bright red crystalline substance; $[(C_7H_6NO_4)_2TeBr_6{\cdot}4H_2O]$ (1015). Yield: 0.467 g (93% based on tellurium oxide taken). Melting point: 415 k (decomposition).

2.2. X-ray crystallography. Powder diffraction

The sample was mounted in a top-loaded sample holder and investigated by X-ray powder diffraction. Powder X-ray data were collected at room temperature using a SIEMENS D5000 diffractometer equipped with a Cu X-ray source employed (λ1 = 1.5406 Å) at 40 kV and 40 mA. In order to limit the axial divergence, 0.02 rad primary and secondary soller slits were inserted.

2.3. Spectroscopic measurements

The infrared spectra of the title complex salts were performed using a Perkin–Elmer 1750 spectrophotometer system with a KBr pellet. The pellet was prepared by mixing 10 mg of powder sample with 200 mg of KBr (The KBr dried at 110 °C) and the whole was compressed into a disk. The $[(C_7H_6NO_4)_2TeBr_6{\cdot}4H_2O]$, pellet was heated in the temperature range 298–473 K; with a heating rate of 20 K/min, in an air-atmosphere Spectac heating cell.

The Raman spectra of crystals were obtained between 303 K and 443 K temperatures with a HoribobinYvan HR800 microcomputer system instrument using a conventional scanning Raman instrument equipped with a Spex 1403 double monochromator (with a pair of 600 grooves/mm gratings) and a Hamamatsu 928 photomultiplier detector. The excitation radiation was provided by coherent radiation with a He–Neon laser at a wavelength of 633 nm, and the output laser power was 50 mW. The spectral resolution, in terms of slit width, varied from 3 to 1 cm^{-1}.

The optical absorption spectra were measured at room temperature using a T90 + –UV–Vis spectrometer within the range of 200–800 nm. $BaSO_4$was used as a reference material.

2.4. Thermal measurements

TGA measurements were carried out on 5–10 mg using a Perkin–Elmer TGA7 instrument, the analysis was conducted in the temperature range 300–1200 K in a nitrogen atmosphere under a constant flow rate of 10 mL/min.

The DSC calorimeter was a Perkin–Elmer DSC4000 with a 20 mL/min flow of N_2. A sample mass of 2–3 mg and a heating rate of 5 K/min were used.

2.5. Single-crystal X-ray crystallography

The crystal data collection and structure refinement, at room temperature, procedures are given in Table 1. Total reflections were collected with a Bruker APEX II CCD diffractometer, correction was made by Lorentz–Polarization effects and absorption. Unit cell parameters were refined using sets of 949.9 reflections. The crystal data of the complex were collected at 293(2) K. Intensity data were collected in the w-2θ scan mode using graphite monochromatic Mo Kα radiation (0.71073 Å). The crystal structure was solved in the monoclinic symmetry, space group $P2_1/c$.

Table 1 Crystal data and structure refinement for $[(C_7H_6NO_4)_2TeBr_6{\cdot}4H_2O]$ at room temperature.

Formula	$(C_7H_6NO_4)_2TeBr_6{\cdot}4H_2O$
Temperature (K)	293(2)
Space group	$P2_1/c$
a (Å)	8.875(5)
b (Å)	15.174(5)
c (Å)	10.199(5)
V (Å^3)	1369.7(1)
Z	2
Dx	2.457
Crystal shape	Monoclinic
F(0 0 0)	949.9
$R(F)$[a]	0.0529
WR_2[b]	0.1530
Goof	0.992

[a] $R = \sum ||F0| - |Fc|| / \sum |F0|$.

[b] $WR_2 = \left[\frac{\sum [w(|Fo|^2 - |Fc|^2)]^2}{\sum [w(|Fo|^2)]^2}\right]^{\frac{1}{2}}$.

Please cite this article in press as: S. Smaoui et al., Synthesis, spectroscopic, structural and thermal characterizations of $[(C_7H_6NO_4)_2TeBr_6{\cdot}4H_2O]$, Journal of Saudi Chemical Society (2016), http://dx.doi.org/10.1016/j.jscs.2016.02.002

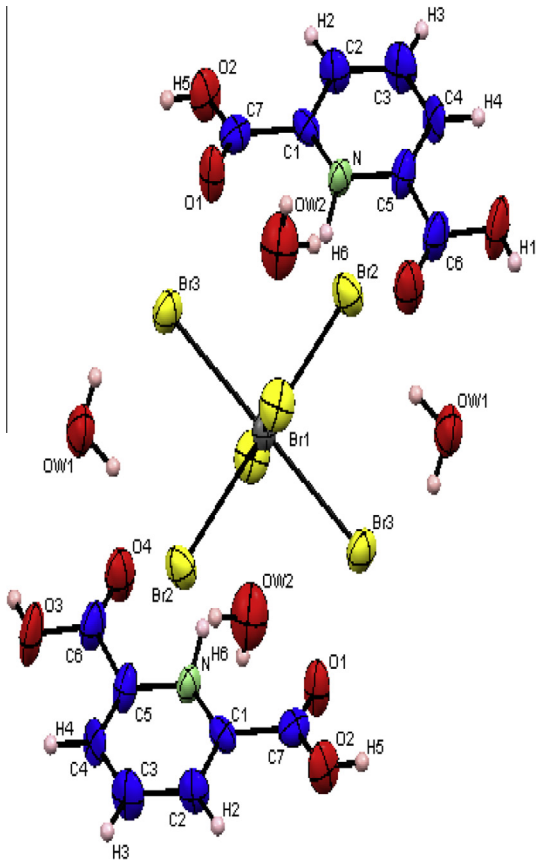

Figure 1 ORTEP view of asymmetric unit in $(C_7H_6NO_4)_2TeBr_6{\cdot}4H_2O$.

The positions of the tellurium atoms were determined through a three dimensional Patterson synthesis. Bromine, carbon, nitrogen and hydrogen atoms were located by a three-dimensional Fourier function. Structure solution and refinement were carried out using SHELX programs [33,34]. The non-hydrogen atoms were refined anisotropically. The hydrogen atoms were attributed to isotropic thermal factors close to those of the atoms to which they are linked.

All the hydrogen positions of the protonated cation were placed geometrically and held in the riding mode (the C–H and O–H bonds were fixed at 0.93 Å and 0.82 Å respectively). The H-atom of the N is located by difference Fourier synthesis.

The atomic coordinates and equivalent isotropic and anisotropic thermal agitation factors are listed in tables (see ESI). The structural graphics of the asymmetric unit were realized with ORTEP [35] and Mercury [36] and the remaining figures were issued by the DIAMOND program [37].

CCDC 1450634 contains the supplementary crystallography data for $[(C_7H_6NO_4)_2TeBr_6{\cdot}4H_2O]$. This data can be obtained free of charge via http:// www.ccdc.cam.ac.uk/conts/retrieving.html, or from the Cambridge Crystallographic Data Centre, 12 Union Road, Cambridge CB2 1EZ, UK (Fax: (international): +441223/336033; e-mail: deposit@ccdc.cam.ac.uk).

3. Results and discussion

3.1. Chemical analysis

The formula $[(C_7H_6NO_4)_2TeBr_6{\cdot}4H_2O]$ was determined by the refinement of the crystal structure at room temperature, it was

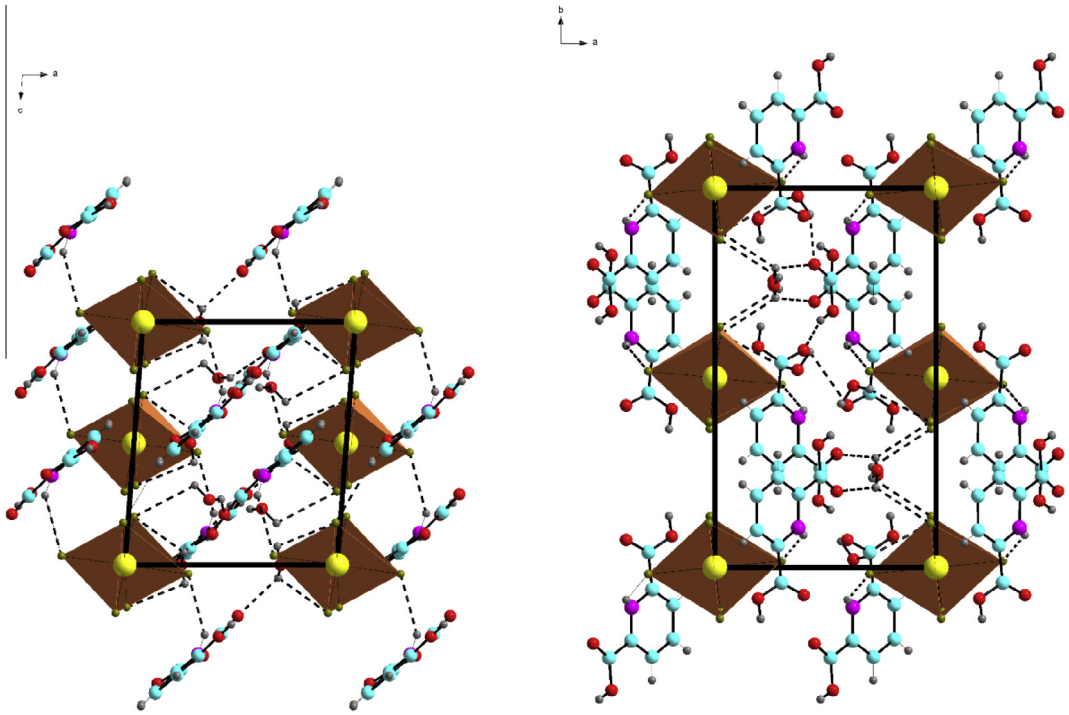

Figure 2 Projection along the *b*-axis and *c*-axis of the structure in $(C_7H_6NO_4)_2TeBr_6{\cdot}4H_2O$. The drawing shows the intermolecular hydrogen bond contacts represented by dotted line.

Table 2 Main interatomic distances (Å) and bond angles (°) involved in hydrogen bonds (e.s.d. are given in parentheses).

D—H···*A*	*D*—H	H···*A*	*D*···*A*	*D*–H–*A*
N–H6···Br1	0.888	2.865	3.653	148.70
O3–H1···O1^{iii}	0.82	1.86	2.657 (1)	162
O2–H5···Ow1^{iv}	0.82	1.74	2.546 (1)	165
Ow1–Hw11···Br2^{v}	0.98 (1)	2.80 (1)	3.523 (9)	131 (8)
Ow1–Hw11···Br3^{vi}	0.98 (1)	2.63 (1)	3.433 (9)	139 (8)
Ow1–Hw12···O3	0.98 (8)	2.43 (1)	3.277 (1)	145 (9)
Ow1–Hw12···O4	0.98 (8)	2.41 (8)	3.353 (1)	161 (9)
Ow2–Hw21···O4	0.98 (9)	2.42 (1)	2.858 (1)	107 (7)
Ow2–Hw21···N	0.98 (9)	1.82 (9)	2.800 (1)	173 (1)
Ow2–Hw22···Br1^{vii}	0.98 (9)	2.57 (9)	3.311 (1)	132 (8)
Ow2–Hw22···O3^{vii}	0.98 (9)	2.55 (1)	3.191 (1)	123 (7)

Symmetry codes: (iii) $-x + 1, y + 1/2, -z + 1/2$; (iv) $-x + 1, -y, -z + 1$; (v) $x + 1, y, z$; (vi) $-x + 1, -y + 1, -z + 1$; (vii) $-x + 1, y - 1/2, -z + 1/2$.

then confirmed by standard tests i.e. Bromine (found 46.12, calcd 47.23%) was determined after hydrolysis by titration with silver nitrate using the potentiometric method. Tellurium (found 10.43, calcd 12.57%) was determined gravimetrically by reduction with SO_2 to the element Te [38]. C, H, N-Analysis, found: C, 16.10; H, 2.01; N, 2.58%. Calc.: C, 16.55; H, 1.97; N, 2.75%.

3.2. Structure determination

At room temperature, $(C_7H_6NO_4)_2TeBr_6{\cdot}4H_2O$ crystallizes in the $P2_1/c$ (N°: 14) monoclinic space group. The structural arrangement is built of isolated $TeBr_6$ octahedra, slightly compressed along the [100] direction, two pydc-2,6 cations and four water molecules. An ORTEP view of the molecule, together with the atomic numbering scheme, is shown in Fig. 1.

The crystalline building stability is ensured by hydrogen bonds N–H···Br, O–H···Br and C═O···H and π stacking interactions join the structural fragments into a three dimensional framework (Fig. 2, Table 2).

The $[TeBr_6]^{2-}$ octahedra are arranged in layers parallel to the (0 0 1) plane in the [$\bar{1}$ 0 1] direction with pydc-2,6 cation interlayers (Fig. 3). The pydc-2,6 cations are orientated in parallel to the plane (5 0 4). The pydc-2,6 cations are multiplied by the symmetry center and translated in the direction of the period b. The distance between the planes of the $[(C_7H_6NO_4)_2TeBr_6{\cdot}4H_2O]$ rings of the adjacent cations is 3.604 Å, and the

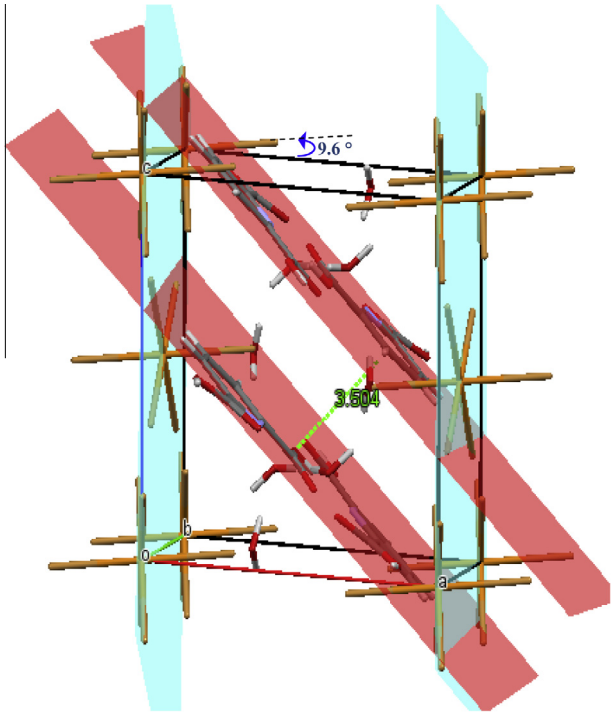

Figure 3 View of parallel planes of organic and inorganic chains.

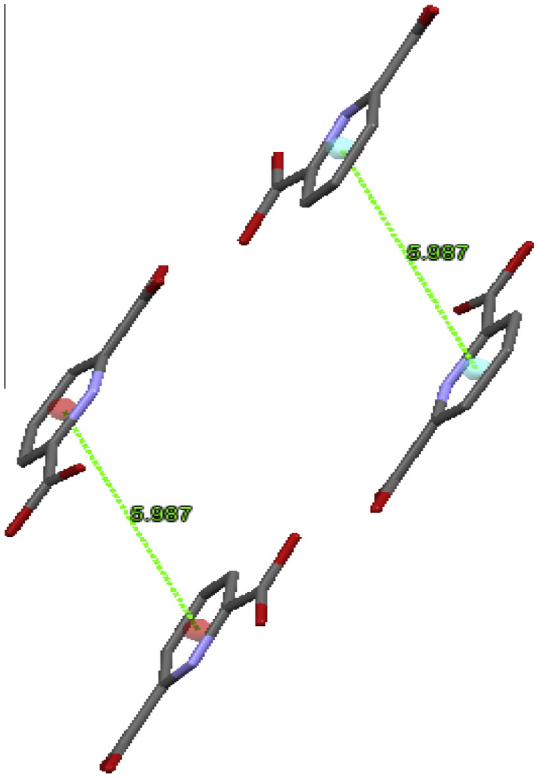

Figure 4 View of the $\pi\ldots\pi$ interactions between ring centroids.

distance between the centroids is 5.987 Å (Fig. 4). The three dimensional framework is built by joining the layers through the Van Deer Walls interactions (see Table 3).

3.3. Environment of Te

The $[TeBr_6]^{2-}$ anions located on an inversion center exhibit a slightly distorted octahedral coordination environment with Te–Br band lengths ranging from 2.6900(2) Å to 2.7025(1) Å (Table 4). The small differences of the Te–Br bond lengths are not significant considering the standard deviations. There appears to be no stereochemical active lone pair of electrons at Te (IV) in the hexahalogeno complex ion [30,31].

The $[TeBr_6]^{2-}$ anions are connected: (i) partly through O–H(w)···Br hydrogen bonds, so an anionic period $[TeBr_6(H_2O)_2]^{2-}$ is formed in the structure (ii) and partly through N–H···Br hydrogen bonds, so the total negative charge (−2) is balanced by the presence of two dependent protonated pydc-2,6 molecules.

The action of the hydrogen bonds N–H···Br1 (N–H 0.888 Å), N···Br1 3.653 Å, H···Br 2.865 Å) and angle NHBr 148.70° leads to a ferrorotative displacement of the $Te–Br_{apical}$ by 9.6° around $\vec{a}$ axis.

3.4. X-ray powder diffraction

The X-ray powder diffraction data were recorded for compound $[(C_7H_6NO_4)_2TeBr_6{\cdot}4H_2O]$ in order to confirm the homogeneity of this compound. The X-ray powder diagrams of the compound resulted in the full indexing of the data and a good agreement between the recorded and calculated peak profiles, indicating that the powder sample of this compound indeed constitute a single phase, as shown in Fig. 5

3.5. Spectroscopic studies at Room temperature

In order to obtain more information on the crystal structure, we studied the vibrational properties using Raman scattering and infrared absorption. In fact, the Raman spectra consist

Table 3 Selected bond distances (Å) and angles (°) of dipicolinic acid in the $[(C_7H_6NO_4)_2TeBr_6{\cdot}4H_2O]$.

Bond length		Bond angle	
C1–N^{ii}	1.350(1)	N^{ii}–C1–C2	121.3(9)
C1–C2	1.369(1)	N^{ii}–C1–C7^{ii}	115.2(9)
C1–C7^{ii}	1.509(2)	C2–C1–C7^{ii}	123.3(1)
C2–C3	1.383(1)	C1–C2–C3	118.1(1)
C3–C4	1.380(1)	C4–C3–C2	119.1(1)
C4–C5^{ii}	1.366(1)	C5^{ii}–C4–C3	120.9(1)
C5–N	1.333(1)	N–C5–C4^{ii}	119.1(9)
C5–C4^{ii}	1.366(1)	N–C5–C6	116.7(9)
C5–C6	1.484(1)	C4–C5–C6	124.1(1)
N–C1^{ii}	1.350(1)	C5–N–C1^{ii}	121.3(9)
C6–O4	1.175(1)	O4–C6–O3	125.8(1)
C6–O3	1.300(1)	O4–C6–C5	123.2(1)
O2–C7	1.302(1)	O3–C6–C5	110.9(1)
C7–O1	1.203(1)	O1–C7–O2	127.2(1)
C7–C1^{ii}	1.509(2)	O1–C7–C1	120.9(1)
		O2–C7–C1^{ii}	111.9(1)

Symmetrycodes: (ii) $-x, -y, -1-z$.

Table 4 Distances (Å) and angles (°) in the anionic tellurium–bromine species, with e.s.d.s in parantheses.

Bond length Te–Br	
Te–Br(1)	2.6900(2)
Te–Br(1)^{i}	2.6900(2)
Te–Br(2)	2.7025(1)
Te–Br(2)^{i}	2.7025(1)
Te–Br(3)	2.7020(1)
Te–Br(3)^{i}	2.7020(1)
Bond angle	
Br(1)^{i}–Te–Br(1)	180.0(5)
Br(1)^{i}–Te–Br(3)	92.48(4)
Br(1)–Te–Br(3)	87.52(4)
Br(1)^{i}–Te–Br(3)^{i}	92.48(4)
Br(3)–Te–Br(3)^{i}	180.0(5)
Br(1)^{i}–Te–Br(2)^{i}	88.44(4)
Br(1)–Te–Br(2)^{i}	91.56(4)
Br(3)–Te–Br(2)^{i}	89.37(5)
Br(3)^{i}–Te–Br(2)^{i}	90.63(5)
Br(1)^{i}–Te–Br(2)	91.56(4)
Br(1)–Te–Br(2)	88.44(4)
Br(3)–Te–Br(2)	90.63(5)
Br(3)^{i}–Te–Br(2)	89.37(5)
Br(2)^{i}–Te–Br(2)	180.0(7)

Symmetrycodes: (i) $-x, -y, -z$.

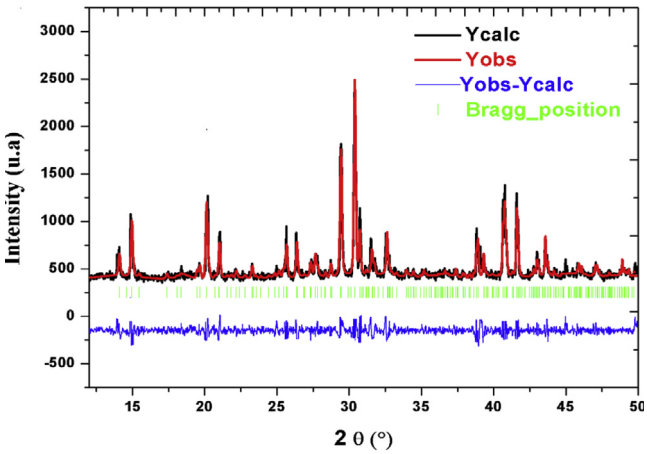

Figure 5 Powder X-ray diffraction pattern and refinement of $(C_7H_6NO_4)_2TeBr_6{\cdot}4H_2O$.

of well-separated peaks that can be subdivided into two main groups presented in Figs. 6 and 7. In fact, in the low frequency range 50–250 cm^{-1}, the Raman bands correspond to the translational, vibrational and external modes of the inorganic groups $[TeBr_6]^{2-}$. As for the bands observed between 250 and 3250 cm^{-1} in the Raman spectra and those in the IR spectra (Fig. 8), they are assigned to the internal modes of the cation. The assignment of the internal and lattice modes of the organic cations and inorganic anion is based on the comparison with the well-documented spectra of the homologous compounds [39–43].

– $[TeBr_6]^{2-}$ anion mode (Fig. 6): The Raman spectrum of this crystal contains two stretching vibrations ν_1 and ν_2 with A_{1g} and E_g symmetries and one bending vibration ν_5 with F_{2g}

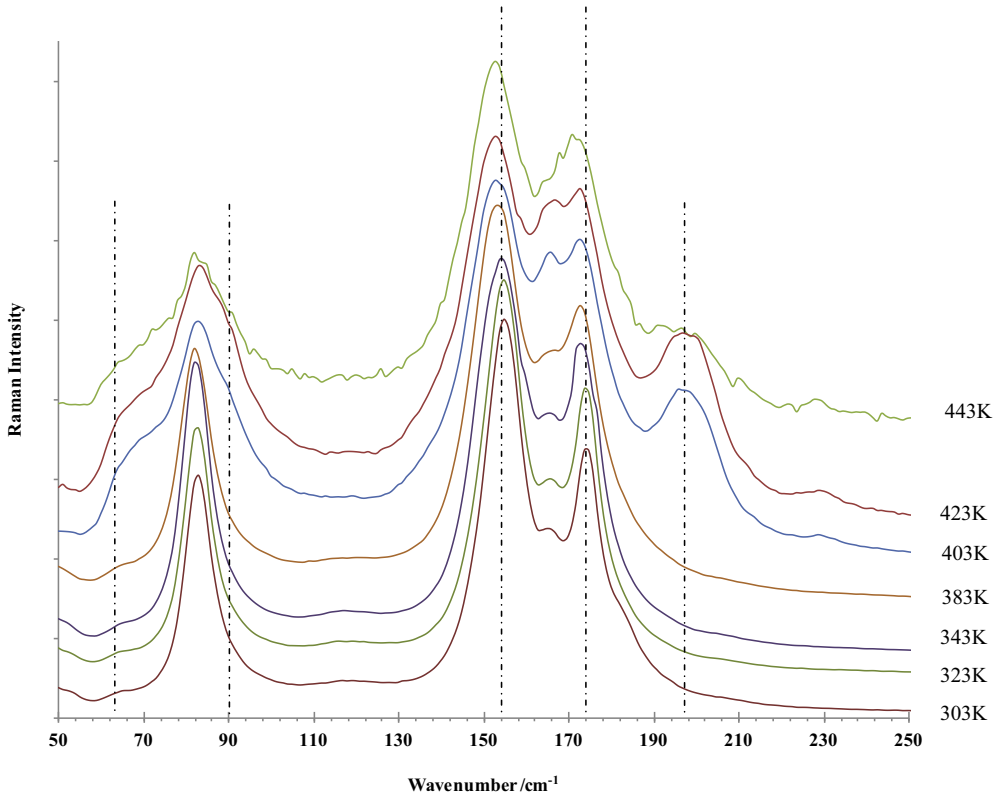

Figure 6 Raman spectra of $[(C_7H_6NO_4)_2TeBr_6{\cdot}4H_2O]$ at different temperatures (frequency range of 50–250 cm^{-1}).

symmetry. Because the $TeBr_6^{2-}$ ion and crystal under study are similar in structure, we can assume that the crystal field does not cause significant distortion of the $TeBr_6^{2-}$ ion and does not break the selection rules for its vibrational spectrum. The crystal filed can give rise to an insignificant frequency shift of the modes, and this is actually observed experimentally. The vibrational mode detected at 175 cm^{-1} could be attributed to the fully symmetric A_{1g} stretching vibration of bromine atoms; the mode at 154 cm^{-1} to the antisymmetric E_g stretching vibration; and the mode at 80 cm^{-1}, to the triply degenerate F_{2g} bending vibration of the $TeBr_6$ group.

Pyridine-2,6-dicarboxylate cation mode (Figs. 7 and 8): the presence of the organic molecule in the compound can be confirmed by a more band absorption in Raman and IR spectra:

- The bands observed in 3450 cm^{-1} are due to N–H stretching vibration in the IR spectrum.
- In aromatic compounds, the C–H stretching wave numbers appear in the range 3000–3100 cm^{-1}. Accordingly, in the present study, the aromatic C–H stretching gives bands at 3080.67 cm^{-1} in the IR spectrum and at 3099.7 cm^{-1} in the Raman spectrum, which correspond to stretching modes of C2–H2, C3–H3, and C4–H4 units.
- Generally, the bands observed in the range 1700–1800 cm^{-1} are due to C═O stretching vibration. This is one of the distinctive features of the carboxylic groups. Accordingly, in the present study, the strong band is revealed at 1744.31 cm^{-1} in the IR spectrum and at 1715 cm^{-1} in the Raman spectrum.
- The strong absorption bands are detected at 1600.93 cm^{-1} in the IR spectrum and at 1611 cm^{-1} in the Raman spectrum assigned to ν(C═C) vibrations in the ligand.
- The ring stretching vibrations are very important in the spectrum of pyridine and its derivatives. They highly characterize the aromatic ring itself. The aromatic ring carbon–carbon stretching vibrations occur in the region 1430–1625 cm^{-1}. In the present work, the C–C aromatic stretch is observed in the region 1400–1580 cm^{-1} in the FT-IR and FT-Raman spectrum.
- The band observed at 1397 cm^{-1} in FT-IR and at 1335.76 cm^{-1} in the Raman spectrum is assigned to C–N stretching vibration [44].
- The IR and Raman bands from 1240 cm^{-1} to 1010 cm^{-1} are due to O─C═O in plane bending and C═O stretching vibrations.
- Below 1000 cm^{-1} several characteristics in plane deformations β(C–H), out-of-plane γ(C–H) and φ(CCC) vibrations as well as out-of-plane (CCC) deformations take place.

Water molecule deformation modes: the presence of water molecules and carboxylic acid stretching in the structure of the complexes is confirmed by broad band at 3500 cm^{-1} arising from the stretching vibrations of ν(OH) groups engaged in hydrogen bands. This band is weak in the Raman spectrum, so IR data are generally used (Fig. 8).

3.6. Spectroscopic effects of hydrogen bonding interactions

As discussed above, the intermolecular and intramolecular hydrogen bonding between pydc-2,6 molecules or with

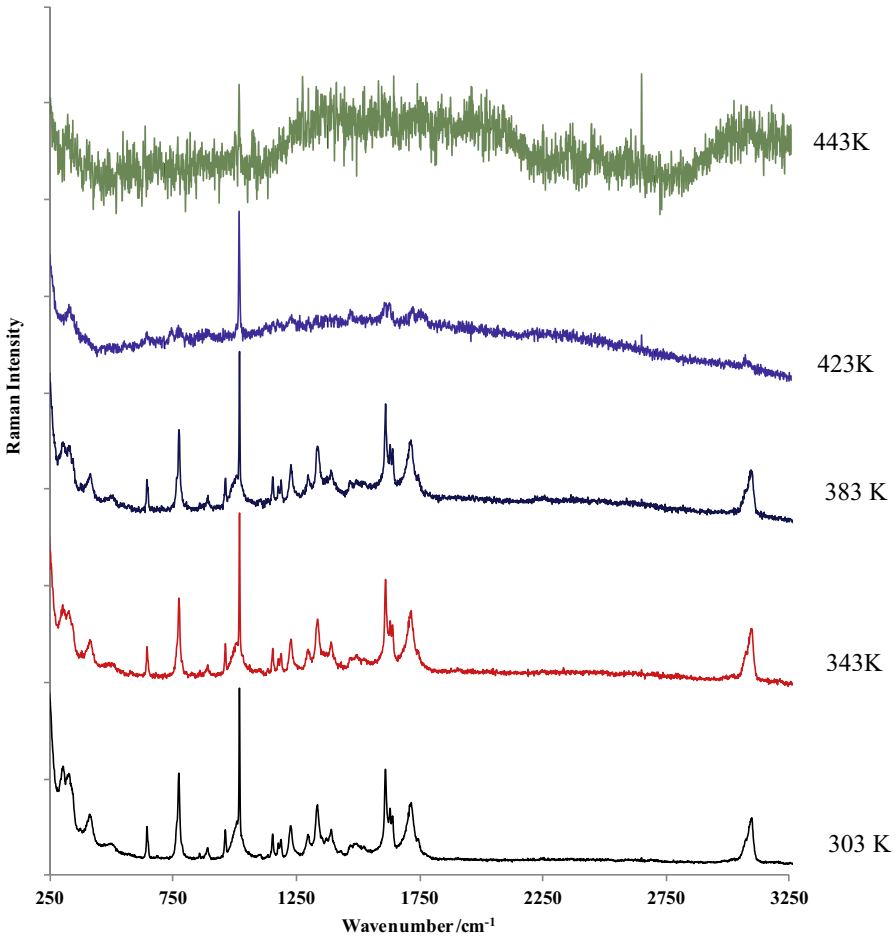

Figure 7 Raman spectra of $[(C_7H_6NO_4)_2TeBr_6{\cdot}4H_2O]$ at different temperatures (frequency range of 250–3550 cm^{-1}).

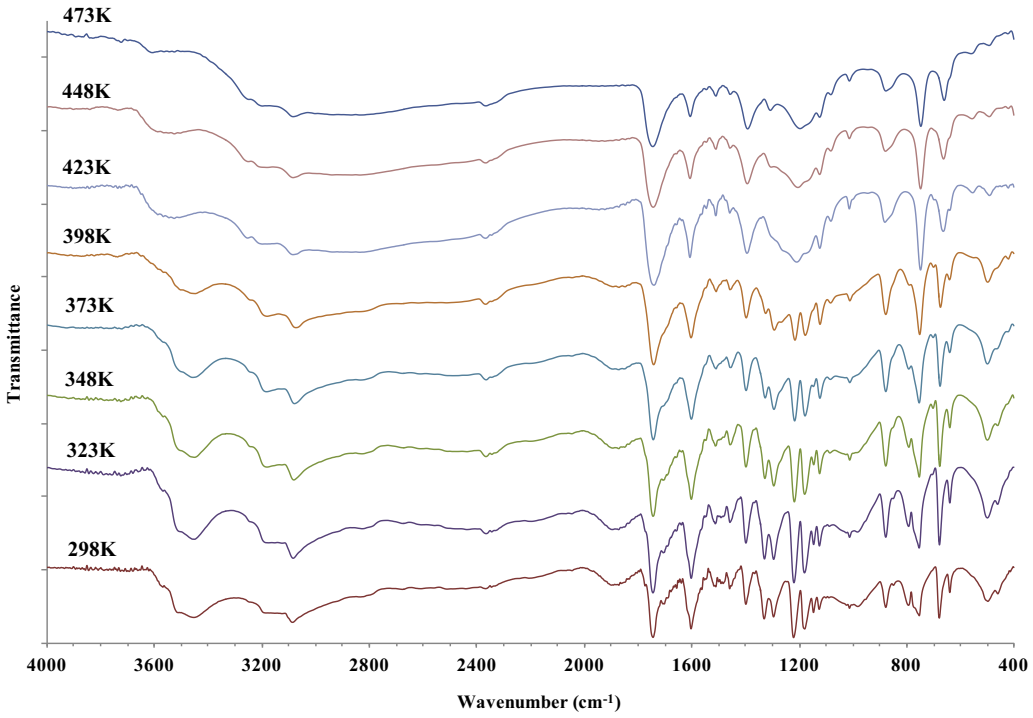

Figure 8 FTIR spectra at different temperatures in the [4000–400] cm^{-1} range of $[(C_7H_6NO_4)_2TeBr_6{\cdot}4H_2O]$ compound.

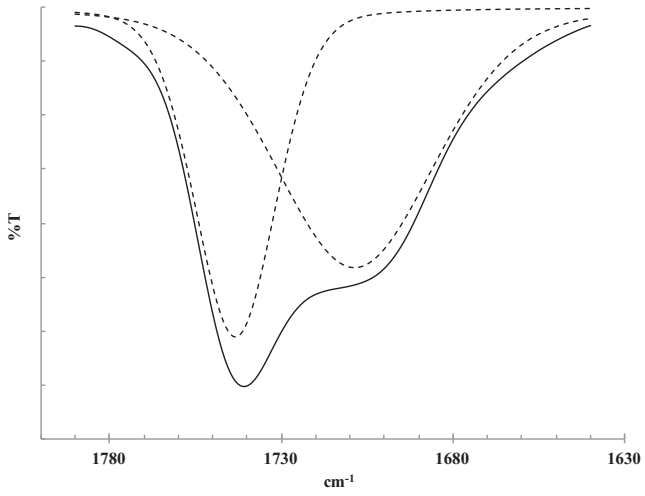

Figure 9 C═O band deconvolution of $[(C_7H_6NO_4)_2TeBr_6{\cdot}4H_2O]$ (1630–1800 cm^{-1} region).

$[TeBr_6]^{2-}$ and water can significantly affect the spectra of pydc-2,6 [45]:

- The C═O region vibration: We fit the C═O bands for the sake of a better understanding. Fig. 9 shows the presence of two peaks at 1742 cm^{-1} and 1706 cm^{-1}. This confirms the presence of hydrogen bond interaction with the carboxyl group (C═O···H).
- The peak centered at 1200 cm^{-1} is assigned to the stretching mode of the O···H···N. These results mean that the intermolecular hydrogen bonding between the pyridyl and the carboxylic acid, especially the new band centered at 1900 cm^{-1} can be seen very clearly. These two new bands are a strong evidence of the intermolecular hydrogen bonding, which is of a unionized type between the pyridyl and the carboxylic acid [46–48]. In order to investigate the thermal stability of the hydrogen bonding and the molecular structure changes at different temperatures, we studied the crystal compound using the temperature-dependent FT-IR and FT-Raman spectroscopy. The temperatures change from 298 K to 473 K.

3.7. Thermal behavior spectroscopy

Fig. 8 shows the temperature-dependent FT-IR spectra of the complex in the region 4000–400 cm^{-1} in the temperature range 298–473 K. The IR spectra show a gradual and continuous decrease in the average hydrogen bonding absorbances at 1940 cm^{-1}, 1705 cm^{-1} and 1200 cm^{-1} as the temperature is increased. Such a temperature effect on the hydrogen bonding has previously been observed in other pyridyl-carboxylic acid systems [49]. The intensity of the large band assigned to ν(O–H) stretching modes centered at 3500 cm^{-1} decreases and the band disappears when temperature increases; which indicates that the water molecules have disappeared and the hydrogen bonds in the structure of the complex were fragilized. These results show that, as the temperature increases, the intermolecular hydrogen bonding deteriorates, but the intramolecular hydrogen bond becomes stable enough to persist to some extent.

A progressive variation of the speed of FTIR and Raman spectra was detected between temperatures 423 K and 473 K. We also report the displacement of certain peaks and the disappearance of others along the frequency field, which indicates

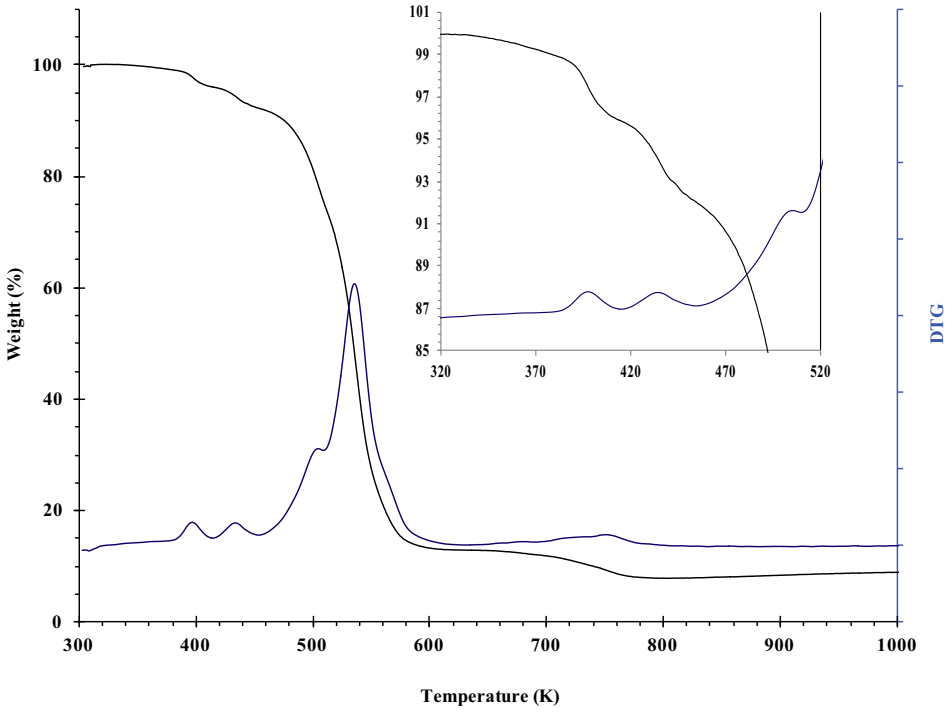

Figure 10 TG/DTG curves of the thermal decomposition of $[(C_7H_6NO_4)_2TeBr_6{\cdot}4H_2O]$ for heating-up run at room temperature.

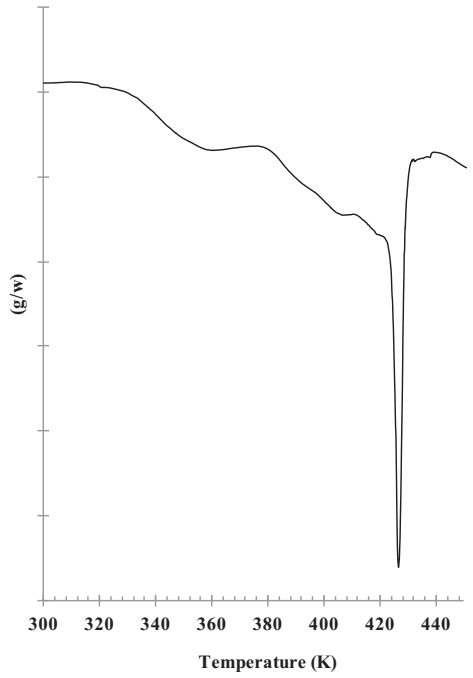

Figure 11 DSC thermogram of $[(C_7H_6NO_4)_2TeBr_6{\cdot}4H_2O]$ in the temperature range 300–460 K.

the departure of an element of the structure. Up to 473 K, the decomposition of the organic molecule occurred; which is confirmed by the total absence of organic molecule bands on the Raman spectrum (Fig. 7).

The anionic vibrations are also affected by the dehydration (Fig. 6) since when the temperature reaches 383 K, the internal modes corresponding to Te–Br stretching show: (i) a sharp decrease in the intensity, (ii) an important increase in the line and (iii) a lower wave number. These phenomena indicate a distortion of $TeBr_6$ octahedra. In fact, the Te–Br terminal and the Te–Br bridging stretching vibrations are sensitive to the dehydration of $[(C_7H_6NO_4)_2TeBr_6{\cdot}4H_2O]$ crystal.

3.8. Thermal property

Figs. 10 and 11 show the TGA-DTG and DSC measurements of the complex $[(C_7H_6NO_4)_2TeBr_6{\cdot}4H_2O]$ respectively. The thermal treatment was carried out to characterize the thermal stability of this compound.

The dehydration process of the $[(C_7H_6NO_4)_2TeBr_6{\cdot}4H_2O]$ complex occurs in two steps in the temperature range 380 K and 450 K as can be seen from Fig. 10. The first mass loss corresponds to the evolution of two water molecules, (found 3.6%, calcd. 3.55%). The next dehydration corresponds to a slow evolution of two water molecules, (found 4%, calcd. 3.55%). The stepwise dehydration processes indicate different strengthes of water molecule bonds. The DSC effect corresponding *t* other water molecules departure process is overlapped by two endothermic effects observed in temperature range 330 K and 410 K. It can be concluded that water molecule bonding liberated at lower temperatures are in the outer coordination sphere, being hydrogen bonded with the complex structure while the water molecules released at higher temperatures are more tightly bonded with metal ions. So, the departure of the organic molecule and the beginning of anion decomposition of the complex are observed in TGA with two successive mass losses at 500 K and 540 K respectively. An endothermic DSC peak at 430 K corresponds to the melting process of $[(C_7H_6NO_4)_2TeBr_6{\cdot}4H_2O]$. This study is in agreement with the results found by the FTIR and Raman spectroscopy (see Fig. 12).

3.9. Optical study

The UV–Vis–NIR diffuse reflectance spectrum of $[(C_7H_6NO_4)_2TeBr_6{\cdot}4H_2O]$ in the region 200–800 nm was studied. The spectra were plotted according to the Kubelka–Munk

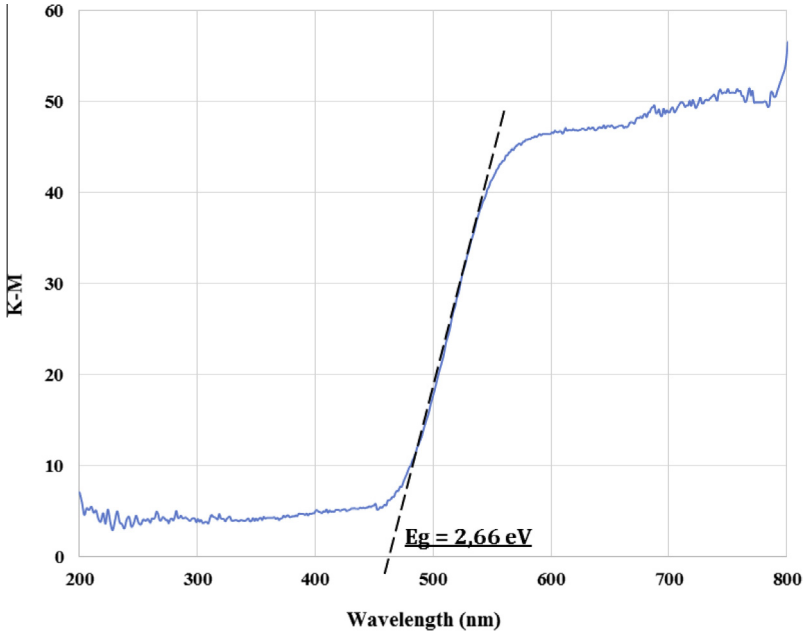

Figure 12 UV/Vis–NIR diffuse reflectance spectroscopy of $[(C_7H_6NO_4)_2TeBr_6{\cdot}4H_2O]$.

function K–M (Fig. 12) [50]. In a K–M versus λ (nm) plot, extrapolating the linear part of the rising curve to zero provides the onset of absorption at 2.66 eV for $[(C_7H_6NO_4)_2TeBr_6{\cdot}4H_2O]$. The reflectance spectrum measurement shows that this compound is a semiconductor material.

4. Conclusion

Single crystals of $[(C_7H_6NO_4)_2TeBr_6{\cdot}4H_2O]$ were collected from an aqueous solution by a slow evaporation technique. This compound belongs to the monoclinic system with $P2_1/c$ space group. The structure of this compound consists of isolated H_2O, isolated $[TeBr_6]^{2-}$ octahedral anions and pydc-2,6 cations. Intermolecular N–H···Br and O–H···Br hydrogen bonds and π–π stacking interactions seem to be effective in the stabilization of the crystal structure. The study of the vibration spectroscopy by FTIR, Raman at room temperatures proves the homogeneity and purity of this synthesis. Crystals of $[(C_7H_6NO_4)_2TeBr_6{\cdot}4H_2O]$ undergo three endothermal peaks at 330 K, 410 K and 430 K which could be explained by the disappearance of the water molecule of the structure and the melting process of crystal respectively. The UV–Vis diffuse reflectance spectrum shows that this compound exhibits semiconducting behavior with an optical band gap of 2.66 eV.

Appendix A. Supplementary data

Supplementary data associated with this article can be found, in the online version, at http://dx.doi.org/10.1016/j.jscs.2016.02.002.

References

[1] D.B. Mitzi, Prog. Inorg. Chem. 48 (1999) 1.
[2] M. Ben Gzaiela, A. Oueslatia, I. Chaabanea, A. Buloub, F. Hlela, M. Gargouria, Spectrochim. Acta Part A Mol. Biomol. Spectrosc. 145 (2015) 223.
[3] L. Carlucci, G. Ciani, D.M. Proserpio, Cryst. Growth Des. 5 (2005) 37.
[4] L. Carlucci, G. Ciani, D.M. Proserpio, Chem. Commun. (2004) 380.
[5] L. Carlucci, G. Ciani, D.M. Proserpio, L. Spadacini, Cryst. Eng. Commun. 6 (2004) 96.
[6] G. Marin, V. Tudor, V.Ch. Kravtsov, M. Schmidtmann, Y.A. Simonov, A. Muller, Cryst. Growth Des. 5 (2005) 279.
[7] R.H. Wang, L. Han, F.L. Jiang, Y.F. Zhou, D.Q. Yuan, M.C. Hong, Cryst. Growth Des. 5 (2005) 129.
[8] B.J. Prince, M.M. Turnbull, R.D. Willett, J. Coord. Chem. 56 (2003) 441.
[9] R.D. Willett, S.F. Haddad, B. Twamley, Acta Crystallogr. C56 (2000) 437.
[10] Li Yamin, Jin Linyu, J. Clust. Sci. 22 (1) (2011) 41.
[11] C. Ma, C. Chen, Q. Liu, D. Liao, L. Li, Eur. J. Inorg. Chem. 1 (2003) 1227.
[12] M. Ranjbar, H. Aghabozorg, A. Moghimi, Acta Crystallogr. Sec. E. 58 (2002) m304.
[13] M. Devereux, M. McCann, V. Leon, V. McKee, R.J. Ball, Polyhedron 21 (2002) 1063.
[14] C.B. Ma, C.N. Chen, Q.T. Liu, Acta Crystallogr. Sec. C 58 (2002) 553.
[15] M. Koman, M. Melnik, M. Moncol, T. Glowiak, Inorg. Chem. Commun. 3 (2000) 489.
[16] R. Jakubas, Structure and Phase Transitions in Alkylammonium Halogenoantimonates(III) and Bismuthates (III), Wroclaw University Press, Wroclaw, 1990.
[17] J. Zaleski, Structure, Phase Transitions and Molecular Motions in Chloroantimonates(III) and Bismuthates(III), Opole University Press, Opole, 1995.
[18] L. Sobczyk, R. Jakubas, J. Zaleski, Pol. J. Chem. 71 (1997) 265.
[19] G. Bator, Dielectric Relaxation and IR Studies on Phase Transitions in Alkylammonium Halogenoantimonates(III) and Bismuthates(III), Wroclaw, 1999.
[20] Taschenbuch. D'Ans-Lax, Für Chemiker und Physiker, Springer-Verlag, Berlin, 1970, Vol. III.
[21] E.J. Lisher, N. Cowlam, L. Gillott, Acta Crystallogr. B 35 (1979) 1033.
[22] J. Dimitropoulos, F. Borsa, Rev. B 41 (1990) 3914.
[23] M. Pragert, A.M. Raaen, I. Svaret, J. Phys. C Solid State Phys. 16 (1983) 181.
[24] R. Karray, A. Kabadou, M. Loukil, A. Ben Salah, Z. Kristallogr, New Cryst. Struct. 218 (2003) 399.
[25] R. Karray, A. Kabadou, I. Cisarova, R. Ben Hassen, A. Ben Salah, J. Alloys Compd. 377 (2004) 85.
[26] W. Ben Aribia, M. Abdelmouleh, R. Karray, A. Van Der Lee, A. Kabadou, A. Ben Salah, J. Mol. Struct. 986 (2011) 86.
[27] M. Loukil, A. Ben Salah, A. Kabadou, J. Alloys Compd. 488 (2009) L10.
[28] F.J. Berry, G. Wilkinson, R.D. Gillard, J.A. McCleverty (Eds.), Comprehensive Coordination Chemistry, vol. 3, Pergamon Press, Oxford, 1987 (Chapter 29).
[29] K. Seppelt, Comments Inorg. Chem. 12 (1991) 199.
[30] R.J. Gillespie, Chem. Soc. Rev. 21 (1992) 59.
[31] S.W. Ng, J.J. Zuckerman, Adv. Inorg. Chem. Radiochem. 29 (1985) 297.
[32] D.J. Stufkens, Recl. Trav. Chim. 89 (1970) 1185.
[33] G.M. Sheldrick, SHELXS97, Program for the Refinement of Crystal Structures, Univ. of Gottingen, Germany, 1986.
[34] G.M. Sheldrick, SHELXL97, Program for the Refinement of Crystal Structures, Univ. of Gottingen, Germany, 1997.
[35] L.J. Farrugia, J. Appl. Cryst. 30 (1997) 565.
[36] C.E. Macrae, I.J. Bruno, J.A. Chisholm, P.R. Edgington, J.Mc. Cabe, E. Pidcock, L. Rodriguez-Monge, R. Taylor, J. Van de Streek, P.A. Wood, J. Appl. Cryst. 41 (2008) 466.
[37] K. Brandenburg, Diamond Version2.0 Impact Gbr, Bonn, Germany, 1998.
[38] L.R. Williams, R. Haskettl, Anal. Chem. 41 (1969) 1138.
[39] A. Nataraj, V. Balachandran, T. Karthick, M. Karabacak, A. Atac, J. Mol. Struct. 1027 (2012) 1.
[40] P. Koczon, J.cz. Dobrowolski, W. Lewandowski, J. Mol. Struct. 655 (2003) 89.
[41] M. Hamdouni, S. Walha, A. Kabadou, C. Duhayon, J. Pascal, Growth Des. 13 (2013) 5100.
[42] R. Lyszczek, J. Anal. Appl. Pyrolsis 86 (2009) 239.
[43] V.A. Stefanovich, L.M. Suslikov, Z.P. Gad'mashi, E.Yu. Peresh, V.I. Sidei, O.V. Zubak, I.V. Galagovets, Phys. Solids State. 46 (2004) 1024.
[44] N. Sundaraganesan, C. Meganathan, B. Ananda, B. Dominic Joshua, Christine Lapouge, Spectrochim. Acta 67 (2007) 830.
[45] K. McCann, J. Laane, J. Mol. Struct. 890 (2008) 346.
[46] T. Kato, T. Uryu, F. Kaneuchi, C. Jin, J.M.J. Frechet, Liq. Cryst. 14 (1993) 1311.
[47] S.L. Johnson, K.A. Rumon, J. Phys. Chem. 69 (1965) 74.
[48] S.E. Odinokov, A.V. Iogansen, Spectrochim. Acta A 28 (1972) 2343.
[49] U. Kumar, T. Kato, J.M.J. Frechet, J. Am. Chem. Soc. 114 (1992).
[50] J. Kang, Y. Yang, S. Pan, H. Yu, Z. Zhou, J. Mol. Struct. 1056 (2014) 79.